

Localized shear generates three-dimensional chaos

L. D. Smith,^{1,2,*} M. Rudman,¹ D. R. Lester,³ and G. Metcalfe^{4,5,6}

¹*Department of Mechanical and Aerospace Engineering,
Monash University, Clayton, VIC 3800, Australia*

²*CSIRO Mineral Resources, Clayton, VIC 3800, Australia*

³*School of Civil, Environmental and Chemical Engineering,
RMIT University, Melbourne, VIC 3000, Australia*

⁴*CSIRO Manufacturing, Highett, VIC 3190, Australia*

⁵*Department of Mechanical and Product Design Engineering,*

Swinburne University of Technology, Hawthorn, VIC 3122, Australia

⁶*School of Mathematical Sciences, Monash University, Clayton, VIC 3800, Australia*

(Dated: October 30, 2022)

Understanding the mechanisms that control 3D fluid transport is central to many processes including mixing, chemical reaction and biological activity. Here a novel mechanism for 3D transport is uncovered where fluid particles are kicked between streamlines near a localized shear, which occurs in many flows and materials. This results in 3D transport similar to Resonance Induced Dispersion (RID); the new mechanism is more rapid and mutually incompatible with RID. We explore its governing impact with a simple model and model fluid flow. We show that transitions from 1D to 2D and 2D to 3D transport occur based on the relative magnitudes of streamline jumps in two transverse directions.

Understanding the mechanisms that control mixing and transport is essential to many natural and engineered flows. Significant insights into fluid mixing have been gained by application of a dynamical systems approach, termed chaotic advection [1, 2], to a range of flows including biological flows [3], geo- and astro-physical flows [4, 5], and industrial and microfluidic flows [6].

Fluid transport and mixing are well understood in 2D chiefly due to the direct analogy between 2D incompressible flows and Hamiltonian systems [1, 7]. In contrast, much less is known about these mechanisms in 3D flows [8], because (a) the Hamiltonian analogy breaks down at stagnation points [9], and (b) there is an explosion of topological complexity between 2D and 3D space. In particular, little is known about the mechanisms that drive transitions from 1D or 2D transport (where particles are confined to curves or surfaces) to 3D transport, an essential ingredient for complete mixing in 3D systems, e.g. plankton blooms where 3D transport alters macroscopic dynamics [10, 11].

One of the few clearly identified 3D transport mechanisms is Resonance Induced Dispersion (RID) [12–15], where fully 3D transport is produced by localized jumps between 1D streamlines. This mechanism is most clearly described in terms of slowly varying ‘action’ variables I and fast ‘angle’ variables θ . RID occurs in systems with two action and one angle variable, such that the volume-preserving map $\mathbf{x}' = \Phi_T(\mathbf{x})$ corresponding to the solution of the period- T advection equation $\dot{\mathbf{x}} = \mathbf{v}(\mathbf{x}, t)$ is transformed into

$$\begin{aligned} I'_1 &= I_1 + \epsilon g_1(I_2, \theta), & I'_2 &= I_2 + \epsilon g_2(I'_1, \theta), \\ \theta' &= \theta + \Omega(I'_1, I'_2) + \epsilon g_3(I'_1, I'_2) \bmod 1, \end{aligned} \quad (1)$$

where $\epsilon \ll 1$ and $g_{1,2,3}$ respectively represent perturbations of I_1, I_2, θ , corresponding to e.g. weakly iner-

tial flows [16, 17]. When $\Omega(I_1, I_2)$ is irrational, particle trajectories densely fill a 1D streamline and (1) reduces to a 2D Hamiltonian system by averaging over θ [14]. However, when a fluid particle enters a resonance region where $\Omega(I_1, I_2)$ is within ϵ of a rational number, θ slows (in the rationally rotating frame) to $\mathcal{O}(\epsilon)$: averaging breaks down, and fluid particles are no longer confined to streamlines of constant I_1, I_2 . In the resonance region fluid particles can ‘jump’ to a new streamline. Fully 3D transport results from multiple streamline jumps as fluid particles repeatedly visit resonance regions.

In this study we uncover a 3D transport mechanism termed ‘Localized Shear Induced Dispersion’ (LSID), which also causes streamline jumping. Unlike RID, LSID is driven by localized shear parallel to a shear surface \mathcal{S} , either as a sharp (yet smooth) or discontinuous deformation. Such localized smooth deformations can arise in general fluids - e.g. from the opening and closing of valves [18, 19] - and can become discontinuous in shear-banding materials such as colloidal suspensions, plastics, polymers, and alloys [20, 21]. For solid matter, sharp smooth deformations occur in granular flows with thin flowing layers, which become discontinuous in the theoretical limit of an infinitesimal flowing layer [22–27].

In action-angle variables LSID can be represented as

$$\begin{aligned} I'_1 &= I_1 + f_1(I_2, \theta), & I'_2 &= I_2 + f_2(I'_1, \theta), \\ \theta' &= \theta + \Omega(I'_1, I'_2) + \epsilon g_3(I'_1, I'_2) \bmod 1, \end{aligned} \quad (2)$$

where $f_{1,2}$ are functions that represent localized shear parallel to $I_{1,2}$. These functions are $\mathcal{O}(\epsilon)$ everywhere except near the shear surface \mathcal{S} where they are $\mathcal{O}(1)$, and typically change sign as they cross \mathcal{S} . Fluid particles that shadow streamlines of constant $I_{1,2}$ are pushed onto a new streamline by $f_{1,2}$ with each approach to \mathcal{S} , leading

to fully 3D transport over many encounters. Therefore, LSID and RID are mutually exclusive; RID cannot occur near \mathcal{S} as the resulting streamline jump would break the resonance.

Another distinguishing feature of LSID is the short-term predictability of each streamline jump. In LSID the relatively simple nature of $f_{1,2}$ means that each streamline jump can be predicted in the short-term. In contrast, in RID streamline jumps are highly sensitive to particle locations in the resonance region, and hence less predictable in the short-term.

To illustrate the LSID mechanism we consider a 2-action system described by eq. (2) with

$$\begin{aligned} f_1(I_2, \theta) &= a_1 (1 + \sin(2\pi I_2/2)) f[(\theta - 0.5)/\delta] \\ f_2(I'_1, \theta) &= a_2 (1 + \sin(2\pi I'_1/2)) f[(\theta - 0.5)/\delta] \\ \Omega(I'_1, I'_2) &= (I'_1 + I'_2)/2, \end{aligned} \quad (3)$$

where $f_{1,2}$ represent localized shears, generated by $f(x) = \tanh(kx)P(x)$ where $P(x)$ is the Gaussian distribution with mean 0 and standard deviation $1/3$, so that f is odd and close to zero outside the interval $(-1, 1)$. The function $f[(\theta - 0.5)/\delta]$ is shown in Fig. 1(b1,b2) for $\delta = 0.02$ with $k = 5$ (smooth) and $k \rightarrow \infty$ (discontinuous); it is odd about 0.5 and rapidly decays to zero. The magnitudes of the localized shears are controlled by $a_{1,2}$, and ‘sharpness’ is controlled by k . When $a_{1,2}$ are both small no noticeable streamline jumps are produced, resulting in 1D transport [Fig. 1(a,b)]. Increasing only a_1 results in streamline jumping transverse to I_1 and hence 2D transport [Fig. 1(c,d)]. Increasing a_2 also results in streamline jumps transverse to I_2 , and hence 3D transport [Fig. 1(e,f)]. In this case $a_1 = 10a_2$ so the magnitudes of streamline jumps transverse to I_1 are larger than those transverse to I_2 , resulting in slow dispersion transverse to I_2 . Sufficiently large $a_{1,2}$ results in rapid 3D transport and chaos [Fig. 1(g,h)].

An important difference with RID is that under LSID $I_{1,2}$ ‘speed up’ near \mathcal{S} rather than θ ‘slowing down’ near a resonant surface. This means that for LSID less time is required near \mathcal{S} for streamline jumps to occur, and hence 3D transport is more rapid. This is demonstrated in the system (3) by the rapid jumps (occurring after a single iteration) that occur, e.g. jumps of 3% in I_1 occur immediately and almost continuously in Fig. 1(c–f). Compared to RID, the streamline jumps of LSID are faster, occur more frequently, and are more predictable in the short-term.

We shall now look at a model fluid flow which exhibits LSID as a result of discontinuous deformations analogous to Fig. 1(b2) rather than the previous smooth model. The 3D Reoriented Potential Mixing (3DRPM) flow [28–30], consists of a periodically reoriented 3D dipole flow contained within the unit sphere [Fig. 2]. After each time period τ (where $\tau = 1$ is the emptying time of the sphere) the source/sink pair is rotated about the y -axis

by $\Theta = 2\pi/3$, resulting in typical tracer particle trajectories shown in Fig. 2(c) [31]. This flow is a 3D extension of the 2D RPM flow [32–34], which exhibits discontinuous slip deformations local to a curve of Lagrangian discontinuity due to the opening and closing of the dipoles [19]. In 2D these discontinuous deformations significantly alter the classical Lagrangian dynamics that arise under smooth deformations (diffeomorphisms), leading to novel Lagrangian coherent structures [19]. Here we show that Lagrangian discontinuities have an even greater impact in 3D systems, providing a mechanism for 3D transport through LSID.

Similar to the 2D RPM flow, the 3DRPM exhibits Lagrangian discontinuities generated by the opening and closing of the dipoles. Fluid [black rectangle AB in Fig. 3] that straddles the surface of Lagrangian discontinuity \mathcal{S} [orange surface in Fig. 3 given by the set of points that reach the dipole after τ] experiences a slip deformation shown in Fig. 3(a–e). This has two components that give the magnitudes of $f_{1,2}$ in eq. (2), where I_1 is the variable parallel to the surfaces of revolution (about the y -axis) generated by the gray streamlines in Fig. 4(c), and I_2 is perpendicular to these surfaces. In the 3DRPM flow the slip parallel to I_1 is generally larger and is clearly observed in Fig. 3(g). Whereas the smaller slip parallel to I_2 is observed via the disjoint distribution in Fig. 3(f).

Like $a_{1,2}$ in eq. (3), τ acts as the control parameter for LSID in the 3DRPM flow. In the limit as $\tau \rightarrow 0$ the flow is steady with velocity \mathbf{v}_0 , equivalent to all dipoles in all positions open [29, 33], and so admits 1D streamlines. Along each of these streamlines $I_{1,2}$ are almost exactly conserved. At small values of τ , $f_{1,2}$ are $\mathcal{O}(\epsilon)$ everywhere and hence particles closely shadow streamlines of \mathbf{v}_0 , as demonstrated by the Poincaré section in Fig. 4(a) which is analogous to Fig. 1(a,b). Increasing τ leads to increases in the magnitudes of both f_1 and f_2 , demonstrated by Fig. 3(f) compared to Fig. 3(g). As f_1 increases more rapidly than f_2 , this results in approximately 2D transport [Fig. 4(b)] analogous to Fig. 1(c,d), with intrasurface chaos loosely confined to isosurfaces of I_2 . A further increase in τ results in slow dispersion away from isosurfaces of I_2 [Fig. 4(c,d)] analogous to Fig. 1(e,f), and eventually 3D chaos [Fig. 4(e)] analogous to Fig. 1(g,h). Here the rapid streamline jumping produced by LSID is again illustrated, occurring after one full flow period 3τ .

To highlight the dominant role that Lagrangian discontinuities play in generation of 3D transport, we track a set of fluid particles that evenly covers the isosurface $I_2 = 0.5$ [dashed black curve in Fig. 4(c)]. The motion parallel to I_2 after 20 flow periods is shown in Fig. 5(a), revealing a discontinuous distribution comprised of sharp interfaces between positive and negative deviations ΔI_2 . These sharp interfaces correspond exactly to the ‘web of preimages’ of the Lagrangian discontinuity [35] shown as the black curves in Fig. 5(b). The distribution of ΔI_2 also highlights the predictable nature of the streamline

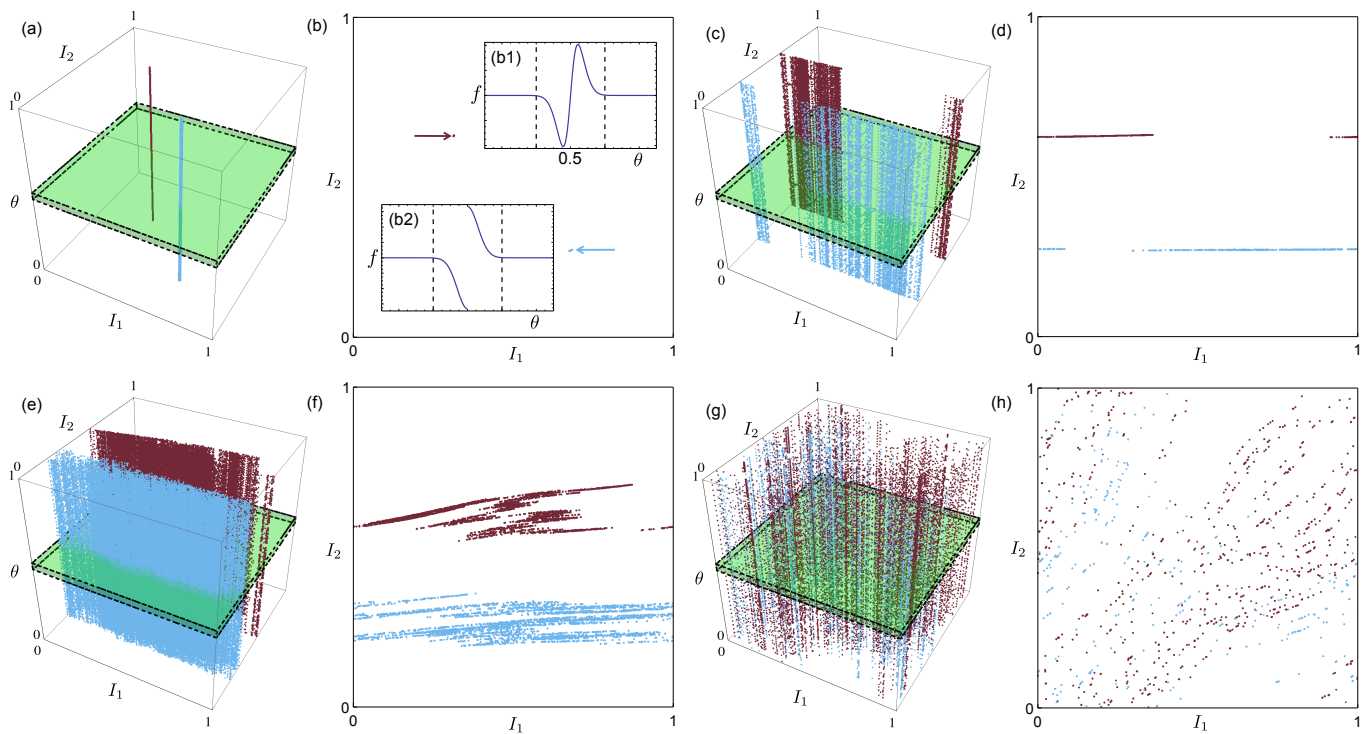


FIG. 1. LSID in the system described by eq. (2) and (3). (a–h) 10^5 iterations of two tracer particles (maroon/dark gray and blue/light gray) for various choices of $a_{1,2}$. Left panels show 3D view with the region $|\theta - 0.5| < \delta$ affected by the shear shown as green. Right panels show projections onto the (I_1, I_2) -plane. (a,b) $a_{1,2} = 5 \times 10^{-4}$. (c,d) $(a_1, a_2) = (0.05, 5 \times 10^{-4})$. (e,f) $(a_1, a_2) = (0.05, 5 \times 10^{-3})$. (g,h) $a_{1,2} = 0.2$. Also shown inset in (b) is $f[(\theta - 0.5)/\delta]$ from eq. (3) [(b1) $k = 5$: smooth, (b2) $k \rightarrow \infty$: discontinuous] shown on the sub-domain $\theta \in [0.45, 0.55]$. The region $|\theta - 0.5| < \delta = 0.02$ is shown by the dashed lines.

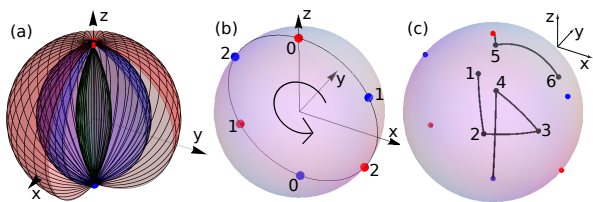


FIG. 2. The 3DRPM flow. (a) Isosurfaces of the Stokes streamfunction of the steady dipole flow. Tracer particles follow streamlines given by the solid curves with constant streamfunction and azimuthal angle. (b) The locations of the source (red) and sink (blue) pairs for the 3DRPM flow with $\Theta = 2\pi/3$. (c) A typical particle trajectory with $\tau = 0.3$.

jumping process over a small number of reorientations, where particles on each side of the web of preimages are driven in opposite directions by $f_{1,2}$ in (2). In the long-term, chaos makes it impossible to predict the transverse motion of particles in LSID, and the associated decorrelation allows the accumulation of jumps to be described as a diffusive-like drift, observed in Fig. 4(c–e).

We have shown that 3D transport can arise via LSID in flows with either smooth or discontinuous deformations in the presence of localized shears that kick particles between streamlines. These deformations can be linked

theoretically by regarding discontinuous deformation as the limit of an increasingly sharp smooth deformation, as demonstrated by f in (3) which is smooth for finite k but discontinuous in the limit $k \rightarrow \infty$ [Fig. 1(b2)]. For switched fluid flows with valves this connection between smooth and discontinuous deformations can be observed by considering different boundary conditions. By replacing the free-slip boundary conditions in the 3DRPM flow with no-slip conditions, fluid would not be cut at the dipole and would remain connected by a thin filament. This means the discontinuous slip deformation is replaced by a localized smooth shear.

Localized shears that occur in a wide array of applications including valved flows, granular flows, and shear-banding materials can produce LSID, a mechanism for 3D particle transport which shares some common features with RID. Under LSID, fluid particles are pushed to a new streamline with each pass of a shear surface, leading to fully 3D transport over the entire chaotic region over many passes near this surface. In both a 2-action model and a valved flow transitions from 1D to 2D transport and 2D to 3D transport result from transitions in the magnitude of streamline jumps in two transverse directions as control parameters increase. Further investigation is required to determine how sharp shears needs

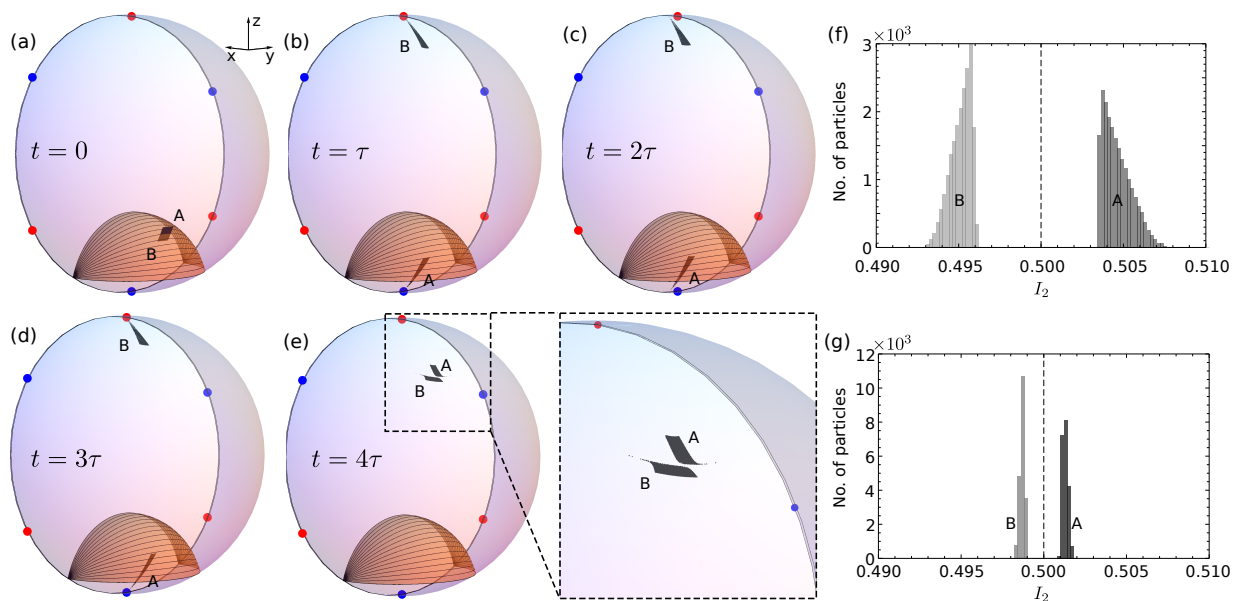


FIG. 3. (a–e) The fluid cutting mechanism in the 3DRPM flow with $\tau = 0.041$. (a) At $t = 0$ a rectangle of black fluid lies on the isosurface $I_2 = 0.5$ and consists of elements A and B which straddle the orange surface consisting of locations that are advected onto the sink at $t = \tau$. (b) At $t = \tau$ the region marked B passes through the dipole and the region marked A does not. (c–d) The dipole is reoriented and the regions A and B move independently. (e) At $t = 4\tau$ the fluid elements A and B approximately recombine, albeit with a discontinuous slip deformation. (f) Histograms of the action variable I_2 for the fluid particles A (dark gray) and B (light gray) shown in (e) at $t = 4\tau$. At $t = 0$ all particles were on the isosurface $I_2 = 0.5$ (dashed black). (g) The same as (f) except with $\tau = 0.01$.

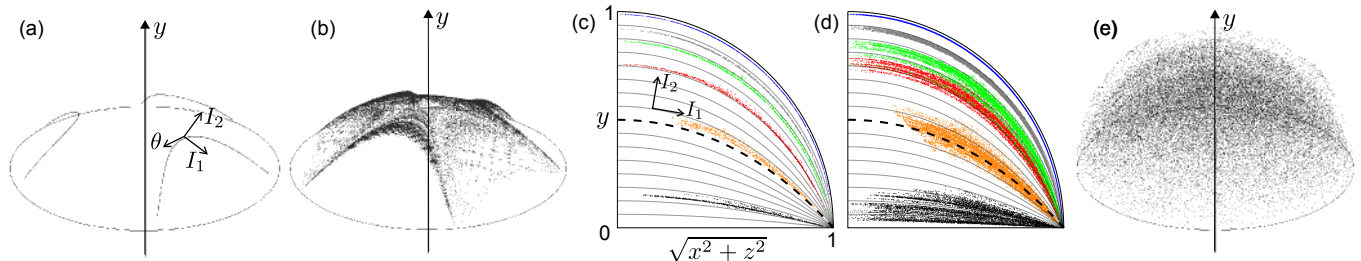


FIG. 4. Typical Poincaré sections for the 3DRPM flow. (a) The orbit of one tracer particle with $\tau = 5 \times 10^{-4}$ after $N = 10^5$ flow periods. (b) $\tau = 0.02$, $N = 10^5$. (c, d) Projections of Poincaré sections (different colors correspond to different initial positions) with $\tau = 0.328$ onto $(\sqrt{x^2 + z^2}, y)$ coordinates. Projections of the isosurfaces of I_2 are shown in gray, and the isosurface $I_2 = 0.5$ is shown as dashed black. (c) $N = 10^3$. (d) $N = 10^4$. (e) $\tau = 5$, $N = 10^5$.

to be to produce LSID. Future studies should also focus on other 2-action systems with localized shears that are likely to experience LSID, to gain a better understanding of the possible transport and mixing phenomena it can produce. For instance, does the rate and type (diffusive, sub-diffusive etc.) of transverse particle drift depend on the nature (e.g. discontinuous, smooth) of the functions f_1, f_2 in eq. (2)?

L. Smith was funded by a Monash Graduate Scholarship and a CSIRO Top-up Scholarship.

ment of Chemical and Biological Engineering, Northwestern University, Evanston, IL 60208, USA.

- [1] H. Aref, *J. Fluid Mech.* **143**, 1 (1984).
- [2] H. Aref, J. R. Blake, M. Budišić, J. H. Cartwright, H. J. Clercx, U. Feudel, R. Golestanian, E. Guillard, Y. L. Guer, G. F. van Heijst, *et al.*, arXiv preprint arXiv:1403.2953 (2014).
- [3] C. López, Z. Neufeld, E. Hernández-García, and P. H. Haynes, *Phys. Chem. Earth Pt. B* **26**, 313 (2001).
- [4] K. Ngan and T. G. Shepherd, *J. Atmos. Sci.* **56**, 4134 (1999).
- [5] S. Wiggins, *Annu. Rev. Fluid Mech.* **37**, 295 (2005).
- [6] N.-T. Nguyen and Z. Wu, *J. Micromech. Microeng.* **15**, R1 (2005).
- [7] J. M. Ottino, *The Kinematics of Mixing: Stretching, Chaos, and Transport* (Cambridge University Press,

* lachlan.smith@northwestern.edu; Now at the Depart-

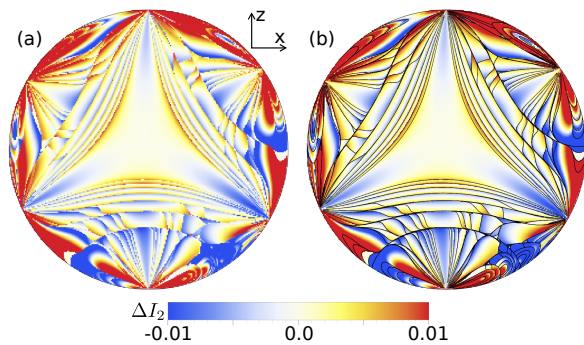


FIG. 5. (a) Transverse displacement of particles evenly distributed on the isosurface $I_2 = 0.5$ in the 3DRPM flow with $\tau = 0.041$ after 20 iterations. This isosurface is projected onto the xz -plane to aid clarity, and each initial particle location is coloured according to the difference in I_2 from 0.5 (ΔI_2). (b) The same as (a) with 20 preimages of the curve given by the intersection of the surface of Lagrangian discontinuity (orange surface in Fig. 3) with the isosurface $I_2 = 0.5$, forming part of the web of preimages of the Lagrangian discontinuity.

- 1989).
- [8] S. Wiggins, *J. Fluid Mech.* **654**, 1 (2010).
- [9] K. Bajer, *Chaos, Solitons & Fractals* **4**, 895 (1994).
- [10] M. Sandulescu, C. López, E. Hernández-García, and U. Feudel, *Ecological Complexity* **5**, 228 (2008).
- [11] T. Tél, A. Moura, C. Grebogi, and G. Károlyi, *Phys. Rep.* **413**, 91 (2005).
- [12] J. H. E. Cartwright, M. Feingold, and O. Piro, *Mixing: Chaos and Turbulence* **373**, 307 (1999).
- [13] D. L. Vainchtein, J. Widloski, and O. Grigoriev, *Phys. Rev. E* **78**, 026302 (2008).
- [14] D. L. Vainchtein and A. Abudu, *Chaos* **22**, 013103 (2012).
- [15] J. D. Meiss, *Commun. Nonlinear Sci. Numer. Simulat.* **17**, 2108 (2012).
- [16] N. R. Moharana, M. F. M. Speetjens, R. R. Trieling, and H. J. H. Clercx, *Physics of Fluids* **25**, 093602 (2013).
- [17] M. F. M. Speetjens, H. J. H. Clercx, and G. J. F. van Heijst, *Phys. Fluids* **18**, 083603 (2006).
- [18] S. W. Jones and H. Aref, *Phys. Fluids* **31**, 469 (1988).
- [19] L. D. Smith, M. Rudman, D. R. Lester, and G. Metcalfe, *Chaos* **26**, 023113 (2016).
- [20] D. V. Louzguine-Luzgin, L. V. Louzguina-Luzgina, and A. Y. Churyumov, *Metals* **3**, 1 (2012).
- [21] P. D. Olmsted, *Rheol. Acta* **47**, 283 (2008).
- [22] G. Metcalfe and M. Shattuck, *Physica* **A233**, 709 (1996).
- [23] J. Ottino and D. Khakhar, *Annu. Rev. Fluid Mech.* **32**, 55 (2000).
- [24] I. C. Christov, J. M. Ottino, and R. M. Lueptow, *Physical Review E* **81**, 046307 (2010).
- [25] G. Juárez, R. M. Lueptow, J. M. Ottino, R. Sturman, and S. Wiggins, *EPL* **91**, 20003 (2010).
- [26] R. Sturman, *Adv. Appl. Mech.* **45**, 51 (2012).
- [27] P. P. Park, P. B. Umbanhowar, J. M. Ottino, and R. M. Lueptow, *Chaos* **26**, 073115 (2016).
- [28] L. D. Smith, M. Rudman, D. R. Lester, and G. Metcalfe, *Chaos* **26**, 053106 (2016).
- [29] L. D. Smith, *Chaotic advection in a three-dimensional volume-preserving potential flow*, Ph.D. thesis, Monash University (2016).
- [30] H. A. Sheldon, P. M. Schaub, P. K. Rachakonda, M. G. Trefry, L. B. Reid, D. R. Lester, G. Metcalfe, T. Poulet, and K. Regenauer-Lieb, *Hydrogeology Journal*, 1 (2015).
- [31] Note that particles that reach the sink are immediately reinjected at the source along the same streamline, as occurs between positions 4 and 5 in Fig. 2(c).
- [32] G. Metcalfe, D. R. Lester, A. Ord, P. Kulkarni, M. Rudman, M. G. Trefry, B. Hobbs, K. Regenauer-Lieb, and J. Morris, *Phil. Trans. R. Soc. A* **368**, 217 (2010).
- [33] D. R. Lester, G. Metcalfe, M. G. Trefry, A. Ord, B. Hobbs, and M. Rudman, *Phys. Rev. E* **80**, 036208 (2009).
- [34] M. G. Trefry, D. R. Lester, G. Metcalfe, A. Ord, and K. Regenauer-Lieb, *J. Contam. Hydrol.* **127**, 15 (2012).
- [35] The set of reverse-time iterates of the Lagrangian discontinuity, giving locations where discontinuous deformation will occur in the future [19].